Transition-Metal Systems in Biochemistry Studied by High-Accuracy Quantum Chemical Methods

Per E. M. Siegbahn and Margareta R. A. Blomberg*

Department of Physics, Stockholm University, Box 6730, S-113 85 Stockholm, Sweden

Received April 30, 1999

Contents

Per E. M. Siegbahn was born in Stockholm, Sweden, did his undergraduate studies at Uppsala University, and received his Ph.D. degree at Stockholm University, 1973 (with Björn O. Roos). He was a postdoctoral fellow at the University of California, Berkeley (with Henry F. Schaefer III) and at IBM, San Jose (with Bowen Liu). He returned to Stockholm University where he became Full Professor in quantum chemistry (1983) and where he has remained ever since. His interests have varied over the years from the development of ab initio quantum chemical methods, to the applications on gas-phase reactions of small molecules, to models of heterogeneous catalysts, to the present main interest in mechanisms for redox-active enzymes.

Margareta R. A. Blomberg received her Ph.D. degree in the field of quantum chemistry at the Department of Physics, Stockholm University, in 1983. After a postdoctorial period at the IBM San Jose research laboratory with Bowen Liu, she returned to Per Siegbahn's group at Stockholm University. Most of her scientific work has been devoted to the elucidation of reaction mechanisms of transition metal systems. In recent years, her research has focused on biochemical systems, in particular metalloenzymes.

I. Introduction

Progress in the area of accurate quantum chemical treatments of systems containing transition metals has been much faster during the past few years than anyone could have expected. Only five years ago, the treatment of the severe dynamical and nondynamical correlation effects seemed almost impossibly difficult even for small transition-metal complexes, and today there are a number of studies using high-accuracy methods of enzyme complexes with models including up to 50 atoms and which contain several transition-metal atoms. A calculation done in 1988 on the low-lying states of the nickel atom[1] is illustrative of the situation at that time. For the nickel atom there are three low-lying states, the $3d^9 4s$, $3d^8 4s^2$ (0.7 kcal/mol) and $3d^{10}$ (40.1 kcal/mol) states, where the experimental (J-averaged) excitation energies are given in parentheses. Since each state has a quite different chemistry, describing the relative positions correctly was considered to be very important. Without correlation, at the Hartree−Fock level but with relativistic effects included, the errors in the splittings are −38.4 and 61.5 kcal/mol, respectively. These huge errors show the difficulties and importance of a correct treatment of dynamical correlation of the 3d shell. Even single-reference coupled-pair functional methods, which are normally quite accurate, gave errors in the splittings of 8.9 and 11.5 kcal/mol. Only

10.1021/cr980390w CCC: $35.00
Published on Web 01/15/2000

a large multireference treatment gave the desired splitting with an error of about 2 kcal/mol, but this type of calculation would be impossible to perform even for a small metal complex. Also, along the same line, work on the chromium dimer showed that errors of more than 1 Å on the bond distance and more than 50% on the binding energy could easily result unless a very elaborate treatment was performed.[2]

There are two main reasons for the surprisingly fast development of accurate treatments of transition-metal systems. The first, and most important, reason is that density functional theory (DFT) has developed into a much more accurate tool than before. In particular, the introduction of terms depending on the gradient of the density to describe the exchange interaction has proven to substantially improve the accuracy.[3,4] This improvement, together with the improvement obtained by introducing a few semiempirical parameters and a part of the Hartree−Fock exchange, has led to an accuracy that is not far away from that obtained by the most accurate ab initio methods at a small fraction of the cost.[5] The second factor responsible for the recent development is simply the increased experience obtained from the large number of model studies of transition-metal complexes performed during the past decade. This experience has, for example, led to a good understanding of how ligands in detail affect chemical reactions and also of how they can be modeled. Another significant insight gained from the modeling of transition-metal complexes is that some of the problems encountered early, which were thought to be necessary to solve, are in fact very atypical for transition-metal complexes. The examples of the nickel atom and chromium dimer given above are illustrative of this point. For an accurate treatment of the bond strength of a small diatomic M−X system, it is often critical that the splittings of the low-lying states of the transition-metal atom M are well described, since the metal commonly changes state as the bond is formed. This is much less critical for the description of the last M−X bond in a saturated MX_n complex, since the atomic state is, in general, the same before and after this bond is formed. In biochemistry it is obviously only the saturated situation that is relevant. Therefore, a DFT method which still has problems describing the lowest states of the metal atom accurately can be quite accurate for a realistic chemical system. In the case of the chromium dimer, the multiple bonding is almost unique with its severe near-degeneracy problems, so this situation does not need to be accurately described by a method used to study more normal chemical systems. Instead, other problems more directly concerned with the modeling of the actual chemical situation become the focus of a theoretical treatment of a transition-metal complex in an enzyme. Some of these problems will be discussed with examples in the present review.

As the title implies, the present review will only be concerned with studies where high-accuracy methods have been used. This category consists of ab initio methods including correlation and DFT methods including gradient corrections. This means that semiempirical studies are not covered, neither are Hartree−Fock studies nor local density studies. In general, these latter methods have been shown to give rather large errors for transition-metal systems. Even for systems containing only atoms from the first and second rows of the periodic table, ab initio methods without correlation and DFT methods without gradient corrections give errors on thermodynamical properties which are at least an order of magnitude larger than those of the more accurate methods. It is therefore rather safe to predict that almost all future studies of biological transition-metal systems will be done using these more accurate methods, even though better parametrizations of semiempirical methods may change this to some extent.

Quantum chemical studies of biological systems have recently been reviewed.[6,7] Of particular relevance for the present review, some transition-metal systems have already been discussed in detail. In order not to make unnecessary repetitions, these systems will not be described again. Instead, these topics and systems will be mentioned here together with the main references. In the previous review, as an example of systems where different ligand models have been tried, tyrosinase and hemocyanin were chosen. There are several quantum chemical treatments of these systems.[8−12] Modelings concerned with accurate geometry determinations were discussed for the case of blue copper proteins.[13,14] Mechanisms were discussed for the case of methane monooxygenase (MMO) for which a few quantum chemical studies have been performed.[15−19] The first preliminary studies of water oxidation in photosystem II were also discussed.[20,21] The present review will instead focus on the more recent work on this subject. Theoretical studies of transition-metal complexes in biochemical systems using high-accuracy methods are still quite rare despite the possibilities provided by the development mentioned above. For example, only a few studies can be found in the literature in the important area of enzyme reaction mechanisms. Therefore, apart from a description of these few studies, examples will also be taken from ongoing research. The examples will serve to illustrate both possibilities and limitations of a theoretical approach to the study of these complicated systems and will give general aspects of the modeling involved. The main examples given will be taken from recent studies on O_2 formation in photosystem II (PSII) and of O_2 activation in cytochrome *c* oxidase (CcO). A major point in the description of these systems, which is given in some detail, is to put the quantum chemical modeling in the context of the very complex overall mechanisms of these enzymes. The number of applications in spectroscopy is somewhat larger although still rather small. The examples discussed below are taken from studies of optical spectra of some copper enzymes and from calculations of spin splittings in some multimetal complexes.

II. Computational Methods

Most studies performed to date on transition-metal complexes in biological systems have been done using DFT methods. The obvious reason for this is the high

efficiency of these methods for large systems. In contrast, there are very few applications using ab initio methods. For example, the highly accurate coupled cluster method, which is routinely used for small organic systems, has so far not been used at all for biochemical transition-metal complexes. However, for spectroscopic applications, CASSCF-based, perturbation theory ab initio methods like CASPT2 have been used in a number of applications. These methods will be very briefly described in the first part of this section. In modeling biochemical reactions it is also important to consider possible effects from the surrounding protein. In most of the studies described below, a simple dielectric medium treatment of the protein is used. This procedure is described in the second part of this section.

A. Quantum Mechanical Methods

The most widely used DFT method for biochemical applications is the B3LYP method.[5,22] The B3LYP functional can be written as

$$F^{\mathrm{B3LYP}} = (1 - A)F_x^{\mathrm{Slater}} + AF_x^{\mathrm{HF}} + BF_x^{\mathrm{Becke}} + CF_c^{\mathrm{LYP}} + (1 - C)F_c^{\mathrm{VWN}}$$

where F_x^{Slater} is the Slater exchange, F_x^{HF} is the Hartree−Fock exchange, F_x^{Becke} is the gradient part of the exchange functional of Becke,[3] F_c^{LYP} is the correlation functional of Lee, Yang, and Parr,[23] and F_c^{VWN} is the correlation functional of Vosko, Wilk, and Nusair.[24] The *A*, *B*, and *C* coefficients were determined[5] using a fit to experimental heats of formation, where the correlation functionals of Perdew and Wang[25] were used instead of F_c^{VWN} and F_c^{LYP} in the expression above. Several DFT functionals, other than B3LYP, have also been used in biochemical applications. The functionals fall into two classes: those that contain Hartree−Fock exchange (hybrid-type methods), such as B3LYP and B3P86, and those that do not, such as BLYP, BP, and BP86.

The accuracy of different DFT methods has been tested on the standard G2 benchmark test[26] consisting of 55 small first- and second-row molecules.[27] A few general conclusions can be drawn from these comparisons. For the atomization energies, the B3LYP method is clearly superior to the other DFT methods with an average deviation to experiments of only 2.20 kcal/mol and a maximum error of 8.4 kcal/mol. This can be compared to the corresponding results of 1.16 and 5.1 kcal/mol, respectively, for the G2 method,[26] which is one of the most accurate ab initio methods available. Of the nonhybrid methods, BLYP performs best with an average deviation of 4.95 kcal/mol and a maximum deviation of 15.8 kcal/mol. It can be noted that both BP and BP86, which are methods commonly used, perform significantly worse with average errors of 11.81 and 10.32 kcal/mol, respectively. Quite surprisingly, bringing in Hartree−Fock exchange for these methods (B3P86) leads only to a marginal improvement to 7.82 kcal/mol. For the geometries of the G2 benchmark test, all DFT methods give quite accurate results, perhaps slightly more accurate for the hybrid methods. It is also worth noting that the geometry convergence with basis set is very fast.

Due to the lack of accurate experimental values, much less is known about the accuracy of DFT methods for transition-metal complexes. However, several systematic theoretical studies have been performed on the small MR^+ systems, where M is a first-row transition metal and R is H, CH_3, CH_2, or OH, and the results were compared to recent experiments.[28] The average absolute error in calculated M−R bond energies is 3.6−5.5 kcal/mol using B3LYP.[29−31] It should be remembered (see introduction) that these systems are some of the most difficult ones to treat since the atomic splittings enter directly into the bond dissociation energies in many cases. For the successive M-CO bond energies in $Fe(CO)_5^+$ and $Ni(CO)_4$ and the first M−CO bond energy in the Cr, Mo, W triad of $M(CO)_6$, B3LYP[29,31,32,36] gives very good agreement with experiment,[33−35,37] with an average error of only 2.6 kcal/mol, and the results are in most cases within the experimental error bars. For the nonhybrid methods, the errors in the calculated M−CO bond energies are in several cases considerably larger. Further indications of this problem were recently given in a study of O−H bond strengths of hydroxyl and water ligands in some manganese complexes,[7] where it was found that the nonhybrid methods gave bond strengths about 20 kcal/mol smaller than those obtained using B3LYP. For the only case where an accurate value is available, $MnO_3(O-H)^-$,[38] the B3LYP result was found to be in good agreement with experiment.

The electronic spectra discussed below were computed using the CASPT2 method.[39] The choice of the active orbital space in the CASSCF calculations is a crucial step. On the basis of experience, it is known that the 10 orbitals representing 3d and 3d′ need to be included in the active space, which is already close to the limit for this method. Normally, other correlations are also important, requiring additional active orbitals, which means that compromises often have to be found. In the calculations on the copper complexes, discussed below, 11 or 12 active orbitals were used.[14] The general strategy for the CASSCF/CASPT2 calculations described here was to first perform a state-averaged CASSCF calculation, where all the excited states of a given symmetry are included in the averaging. In the subsequent CASPT2 step, all valence electrons were correlated including the 3s,3p shell. A level shift was applied to remove the intruder states. Basis sets as large as could be afforded were used, but still, as will be discussed below, significant compromises in the choice had to be made. For example, no polarization functions on C, N, or H were included.

The CASPT2 method is probably the most accurate method available today for calculations of optical spectra. It has been extensively tested on organic systems and typically predicts excitation energies with error bars of 0.3 eV (7 kcal/mol). For small transition-metal complexes, a similar accuracy can also be reached. For larger complexes, particularly those in biochemistry which lack symmetry, the accuracy decreases mainly due to problems in de-

scribing the main chemical effects within an active space limited to about 12 orbitals. As mentioned above, basis set truncations also reduce the accuracy, and this is a much more severe problem in CASPT2 than in DFT calculations since the basis set convergence is much slower.

B. Dielectric Methods

When studying biochemical problems, it is important to also consider the modeling of the part of the enzyme that surrounds the part treated quantum mechanically. There are different degrees of sophistication of this part of the model, ranging from neglect of the surrounding protein, to the use of different levels of dielectric models, to the use of different molecular mechanics (MM) force fields, to the use of a semiempirical description. A major question in this context for metal enzymes concerns the charge state to be used on the active site complex. These questions were discussed in connection to several examples of different modelings in the recent review.[7] Methods which combine quantum chemical and molecular mechanics (QM-MM) methods,[40] have not yet been applied on biological transition-metal systems using DFT or accurate ab initio methods.

The effects of the protein surrounding on structures and on electron-transfer processes have been studied using DFT methods. For blue copper proteins, which until recently have been considered to be classical cases where the protein has a major and decisive effect on the *structure* of a metal complex, a recent study[13] has shown that the effect of the protein surrounding is truly minor. For electron-transfer and charge-separation processes in the bacterial photosynthetic reaction center, another study[41] has shown that a simple structureless dielectric model is sufficient for recovering the major effects of the protein on the transfer energy. Similar conclusions can be drawn from the calculations of redox potentials of superoxide dismutase enzymes discussed below. Although all these studies point in the same direction, that the protein surrounding does not need to be very accurately described, there is not yet a sufficient number of results available to make general conclusions. However, so far there are no known high-accuracy examples which conclusively show the opposite. Furthermore, in most of the mechanistic studies discussed below it is found that when there is no long-range charge separation involved in the reaction, the effects of the surrounding protein on the reaction energetics are generally small.

In most of the mechanistic studies discussed below the effects of the protein were included through the application of a dielectric medium, with the molecule placed in a cavity. In the simplest implementations of this procedure, the shape of the cavity is chosen as a sphere. For reasonably flat molecules, e.g., a pure heme or a chlorophyll molecule, an ellipsoidal cavity represents an important improvement. However, if the heme or chlorophyll molecule has axial ligands, e.g., a histidine coordinating to the central metal atom, it is necessary to use irregularly shaped cavities, which closely follow the shape of the molecule. In such cases the self-consistent isodensity polarized continuum model (SCI−PCM) as implemented in the GAUSSIAN-94[42] program can be used. In this method the solute cavity is determined self-consistently. The default isodensity value of 0.0004e/B^3 has been found to yield volumes very close to the observed molar volumes. The dielectric constant of the protein is the main empirical parameter of the model, and in the studies discussed below, it was normally chosen to be equal to 4, in line with previous suggestions for proteins. This value corresponds to a dielectric constant of about 3 for the protein itself and of 80 for the water medium surrounding the protein. It should, in this context, be noted that with such a simple model of the protein surrounding as a dielectric continuum, it is very important to include the hydrogen bonding to the solute explicitly in the quantum chemical model. The consequence of this type of modeling can be nicely illustrated by the case of the electron affinity for the quinone in the bacterial reaction center. Using a quantum chemical model consisting of the quinone and two water molecules embedded in a continuum with $\epsilon = 4$, an electron affinity of 86.1 kcal/mol is obtained. However, it is generally considered that the region around the quinones in the reaction center is quite polar and therefore has to be described by a high dielectric constant.[43] In fact, using a small quinone model without hydrogen bonding, together with $\epsilon = 80$, gives an electron affinity of 85.0 kcal/mol, very close to the value of 86.1 kcal/mol obtained for the model with hydrogen bonding and $\epsilon = 4$. However, a model treating the most important hydrogen bonding explicitly by quantum chemical methods and assigning a uniform low dielectric constant to the rest of the protein is considered here to be most appropriate. The choice of $\epsilon = 4$ can also be motivated by the fact that this value gives good agreement with experiment for all three charge-separation reactions studied in the photosynthetic bacteriosystem.[4] It was also concluded that directional effects, which have to be modeled by explicitly charged residues, do not appear to be important in this system.

III. Mechanisms

To illustrate what is involved in a theoretical study of a transition-metal-catalyzed enzyme reaction, the present section will concentrate on two different examples which will be described in some detail. These examples are taken from our own ongoing research on two of the most interesting and therefore experimentally most studied enzymes, cytochrome *c* oxidase (CcO) in the respiratory chain and photosystem II (PSII) in green plants, algae, and cyanobacteria. Both involve complexes with several transition-metal centers and the O_2 molecule. In cytochrome *c* oxidase, O_2 is reduced to water and the energy produced is used to make ATP. In this process there is a complicated flow of electrons and protons, and this situation has to be analyzed in detail before proper model calculations can be set up. The first section below will illustrate how this is done in practice and how the vast amount of experimental information is used in this context. In particular, the number of electrons and protons given to the bime-

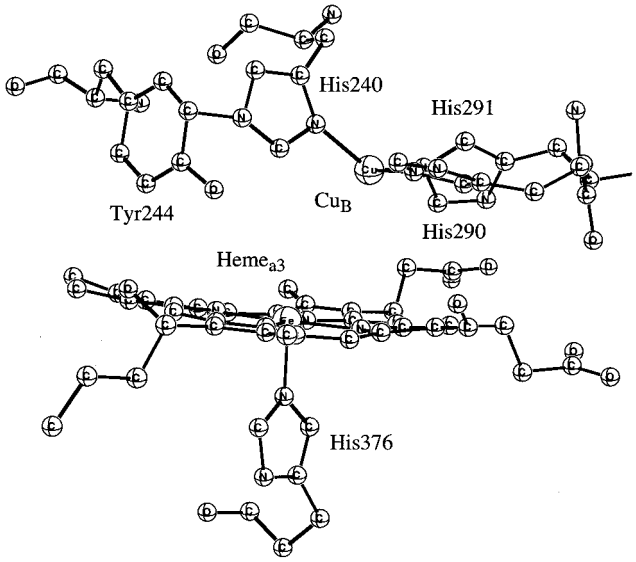

Figure 1. X-ray structure of the binuclear center in CcO (modified to include the His−Tyr covalent link).

tallic active site is absolutely critical if relevant conclusions should be drawn from the calculations. In the second example below, the opposite reaction with the formation of O_2 from water in photosystem II is discussed. A severe complication in such a study is that, thus far, there is no X-ray structure of PSII. The discussion will describe what type of problems can be addressed under such circumstances and how models of the active site can be set up from the present experimental information. Finally, in the third subsection, other enzyme mechanisms involving transition-metal complexes that have recently been studied will be briefly described. Other examples have been recently reviewed.[7]

A. O_2 Activation in Cytochrome *c* Oxidase

The reduction of molecular oxygen to water

$$O_2 + 4H^+ + 4e^- \rightarrow 2H_2O \qquad (1)$$

in cytochrome *c* oxidase (CcO, also called complex IV) occurs at a binuclear metal site, consisting of a heme-iron, $heme_{a3}$, and a histidine-ligated copper center, Cu_B, see Figure 1. The O_2 molecule coordinates to the $heme_{a3}$-iron in the fully reduced form of the enzyme, where it receives electrons and protons from nearby residues. The $heme_{a3}$-iron in the reduced enzyme is Fe(II), and it ends up as Fe(III) after the completed reaction, giving one of the electrons to the O_2 reduction. In the same way, Cu_B goes from Cu(I) to Cu(II). The remaining two electrons needed to fully reduce one molecule of O_2 to two water molecules are transferred to the binuclear site via another heme group, $heme_a$, which is located 13 Å away from the binuclear center (iron to iron distance). The proton-transfer pathways to the active site are also reasonably well-known.[44]

In setting up a model of the binuclear center shown in Figure 1 to perform a quantum chemical investigation of the O_2 activation in CcO, the most difficult part is to know how to treat the electrons and protons in reaction 1. In fact, as shown in the following equation, it is the transfer of these electrons and protons that at the end saves and stores the energy produced in the overall O_2 reduction reaction, eq 2.

$$C_6H_{12}O_6 + 6O_2 \rightarrow 6CO_2 + 6H_2O + \text{energy} \qquad (2)$$

The energy released in this reaction is stored by the organism in the form of ATP. To analyze this fundamental reaction further, it is normally partitioned into two half-reactions:

$$C_6H_{12}O_6 + 6H_2O \rightarrow 6CO_2 + 24H^+ + 24e^- \qquad (3)$$

and

$$6O_2 + 24H^+ + 24e^- \rightarrow 12H_2O \qquad (4)$$

The first of these two reactions (eq 3) occurs in glycolysis and the citric acid cycle and results in the production of NADH and $FADH_2$. Mediated by these coenzymes and a set of redox centers, the electrons and protons are made available for the O_2 reduction in the second reaction, eq 4. This electron transfer, occurring in the mitochondria and driven by the O_2 reduction, creates a proton gradient by pumping protons across the membrane. The proton gradient results in the production of ATP by ATP synthase. The main part of the proton pumping occurs in three electron-transfer proteins, complex I, III, and IV, all located in the mitocondrial membrane. It is only in the last one of these proteins, complex IV (or CcO), that the reduction of molecular oxygen to water takes place. The energy gained in the O_2 splitting drives the electrons through all the electron-transfer proteins, step by step, by means of progressively increasing electron affinities (reduction potentials) of the redox centers located in or between the electron-transfer proteins. A thorough analysis of this process leads to the following important conclusions. Since only a few of the total number of protons pumped in the respiratory chain are pumped locally in CcO and since the energy involved in pumping each proton is rather small (3−5 kcal/mol), most of the energy produced in the O_2 reduction should be used to increase the electron affinity (EA) of the active site. Much less energy should go into increasing the proton affinity. For the modeling of the O−O bond-breaking reaction, this means that the electron coming from outside the binuclear center is *not* likely to be used to activate the bond. It should only come in *after* the reaction is completed. After each step in the O_2 reduction reaction has taken place, the increased electron affinity should be used to drive electrons along the respiratory chain, which in turn will drive protons across the membrane.

In a quantum chemical investigation of the mechanisms for the O_2 splitting, the basic model shown in Figure 2 has been used.[45] The heme group is replaced by an iron with two chelating diformamidate ($NHCHNH^-$) ligands while all histidines, except the one covalently linked to the tyrosine, are replaced by ammonia. In calculations on the separated iron or copper complexes, somewhat larger models could be chosen, using imidazoles for all histidines and a full unsubstituted iron−porphyrin for the heme group.

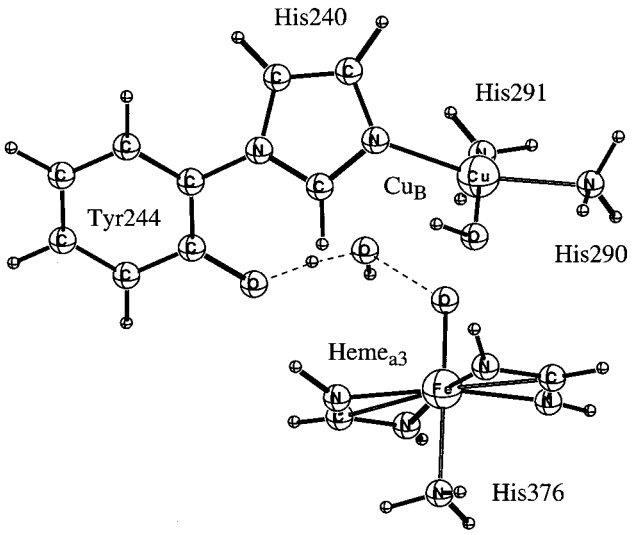

Figure 2. O−O splitting transition state for a model of the binuclear center in CcO.

The number of protons and electrons included in the model can be varied to investigate different aspects of the reaction. For a reaction mechanism to be possible, the following criteria should be fulfilled: (i) each reaction step should be reasonably close to thermoneutral so that it does not waste energy as heat, (ii) there should be no high barrier involved, (iii) the reaction should mainly increase the EA of the active site (see above). On the basis of the different kinds of experimental information, several suggestions have been made for the O_2 reduction mechanism and some of those suggestions have been investigated by performing B3LYP calculations on the type of model described above.

The first step in the O_2 activation is coordination of the O_2 molecule to the Fe(II) center of heme$_{a3}$. In this complex, referred to as compound A, O_2 has been shown to be very weakly bound to the iron.[46] The Fe−O_2 bond energy can be calculated using the large iron−porphyrin model. The ground state is an open-shell singlet state, and at the B3LYP level, this Fe−O_2 bond energy is only 2 kcal/mol, in good agreement with the experimental estimates of a weak bond. The small heme model mentioned above gives a somewhat stronger Fe−O_2 bond, 9 kcal/mol.

The second step in the O_2 activation is the formation of a state labeled compound P. On the basis of its optical spectrum, the electronic structure of this state was interpreted to be (porf)Fe(III)−O−O^-.[46,47] As will be discussed below, however, the structure of the P intermediate is under debate.[48,49] Irrespective of the character of the experimentally observed compound P, the reaction sequence is thought to occur via a peroxy-type structure, and one possible candidate for such a structure is (porf)Fe(III)−O−OH. A water molecule, observed in the vicinity of CuB, could be involved in the formation of the peroxide structure through the donation of a proton to the O_2 molecule coordinated to iron. At the same time, an electron is donated by Cu$_B$, giving an Fe(III)-O−OH + Cu(II)(OH) state of the binuclear center. The energetics of such a reaction is estimated from reaction 5

$$\begin{aligned}&\text{(porf)Fe(II)}-\text{O}_2 + \\ &\qquad [(\text{H}_2\text{O})\text{Cu(I)(His)}_2\text{(His}-\text{TyrOH)}]^+ \rightarrow \\ &\qquad\qquad \text{(porf)Fe(III)}-\text{O}-\text{OH} + \\ &\qquad\qquad [(\text{OH})\text{Cu(II)(His)}_2\text{(His}-\text{TyrOH)}]^+ \quad (5)\end{aligned}$$

which is calculated to be slightly endothermic using the larger models described above at the B3LYP level. The endothermicity of this reaction step could correspond to the experimentally observed barrier for the O_2 splitting on the order of 6 kcal/mol.[50] Whether a barrier exists in excess of the endothermicity of reaction 5 is presently under investigation.

The next step in the reaction is the splitting of the O−O bond, which eventually leads to an oxoferryl intermediate, (porf)Fe(IV)=O. One of the controversies regarding the mechanisms of the O_2 activation in CcO is if the O−O bond splits before or after the arrival of the third electron at the binuclear center, see also the discussion above concerning the coupling between O_2 reduction and electron transfer. It has been suggested on the basis of time-resolved Raman spectroscopy that the peroxide structure is not a stable intermediate and that the O−O bond actually already breaks before the arrival of the third electron.[48,49] This is in contrast to other suggestions that the peroxide-type of structure, (porf)Fe(III)−O−OH, is a true intermediate which requires a third electron to split the O−O bond.[47] Thus, an obvious topic for a quantum chemical study is to investigate the conditions for the O−O bond splitting at the binuclear site in CcO.

The O−O splitting step, without the introduction of the third electron from heme$_a$, could occur via the reaction described in eq 6

$$\begin{aligned}&\text{(porf)Fe(III)}-\text{O}-\text{OH} + \\ &\qquad [(\text{OH})\text{Cu(II)(His)}_2\text{(His}-\text{TyrOH)}]^+ \rightarrow \\ &\qquad\qquad \text{(porf)Fe(IV)}=\text{O}-\text{H}_2\text{O} + \\ &\qquad\qquad [(\text{OH})\text{Cu(II)(His)}_2\text{(His}-\text{TyrO*)}]^+ \quad (6)\end{aligned}$$

Besides the oxoferryl species, (porf)Fe(IV)=O, a water molecule is formed. In this particular reaction scheme, the proton and electron that need to be added to the peroxide, (porf)Fe−O−OH, to form the water molecule are taken from the covalently linked tyrosine, leading to the formation of a neutral tyrosine radical, as previously suggested.[49] Using the type of model shown in Figure 2 and using the B3LYP functional, reaction 6 is calculated to be close to thermoneutral, which shows that it is thermodynamically feasible to break the O−O bond before the third electron arrives at the binuclear center, which is a significant result. However, it should be noted that the exact location of the radical created in this reaction depends on the detailed nature of the model and cannot be inferred from the calculations. Other possible locations, besides the cross-linked tyrosine, are the copper−imidazole complex and the porphyrin ring. All these different locations of the radical hole are close in energy, and the location of the radical is therefore not very energetically significant.

If the splitting of the O−O bond, on the other hand, would occur only after the third electron is intro-

duced, the following reaction scheme (eq 7) could be followed

$$\begin{aligned}&(\text{porf})\text{Fe(III)}-\text{O}-\text{OH} + \\ &\quad (\text{OH})\text{Cu(I)}(\text{His})_2(\text{His}-\text{TyrOH}) \rightarrow \\ &\quad\quad (\text{porf})\text{Fe(IV)}=\text{O}-\text{H}_2\text{O} + \\ &\quad\quad\quad (\text{OH})\text{Cu(II)}(\text{His})_2(\text{His}-\text{TyrO}) \quad (7)\end{aligned}$$

In this case the reaction starts out with Cu(I). Thus, the electron needed for the water formation can be taken from the copper center and no radical needs to be created. Using the model system in Figure 2, reaction 7 is calculated to be more than 30 kcal/mol exothermic. This result rules out this model, since it means that the energy gained in the O−O splitting would be lost into heat. The simplest interpretation of this result is that the third electron cannot be considered as free, which is done in this computation. Thus, the energy released in the O_2 splitting is needed to make the third electron move from heme$_a$ to the binuclear site, and therefore, the O_2 splitting must occur *before* the third electron arrives. The mechanism for turning the energy liberated in the O_2 splitting into a driving force for the electron transport is to generate an increase in the electron affinity of the binuclear site. This increase in the electron affinity can be calculated from reactions 6 and 7, and it is found to be about 30 kcal/mol. Furthermore, when an electron is moved from heme$_a$, an electron can be moved forward over the redox centers in the electron-transport chain, and in this way the energy released in the O_2 reduction, occurring only in CcO, can be used to drive the electrons through all the electron transport complexes. The proton pumping across the membrane, in turn, is achieved through electrostatic effects coupled to the introduction of new electrons into each of the electron-transport complexes.

To summarize, the criterion mentioned above, that each reaction step in the O_2 reduction reaction should be close to thermoneutral, is fulfilled for the O_2 splitting step if it occurs before the arrival of the third electron. The exact location of the radical created in such a reaction cannot be determined from the calculations, since the different options are too close in energy. This result indicates that the location of the radical is of small energetic importance. However, it could still be of some importance for the proton translocation. Furthermore, the O_2 splitting is calculated to create an increased electron affinity of the binuclear center, which can be used to drive the electrons. Finally, the criterion that there should be no high barriers involved has not been discussed so far. It turns out that for the model shown in Figure 2, the barrier for the O−O splitting is too high, more than 20 kcal/mol, calculated at the B3LYP level. Preliminary calculations on slightly more elaborate models of reaction 6 indicate that if the proton that is needed for the water formation is made energetically more easily accessible to the binuclear site, the barrier for the O−O splitting decreases to a reasonable level.

In another recent theoretical study of the binuclear center in CcO,[51] mainly unrestricted Hartree−Fock calculations were performed. Since correlation effects are extremely important for transition-metal systems, the energetic results obtained for the O_2 activation process are not very reliable. For example, it was found that molecular oxygen binds 28 kcal/mol stronger at the copper site than at the iron site, which appears as an unrealistic result. A vibrational analysis of the oxo−ferryl compound F was recently performed at the DFT level using the same type of porphyrin model as that shown in Figure 2, giving some support for the hypothesis that the Fe(IV)=O fragment could be tilted relative to the porphyrin ring.[52]

B. Water Oxidation in Photosystem II

The water oxidizing complex (WOC) in PSII performs a unique chemistry in catalyzing the photochemical formation of O_2 from water using visible light. There is no other system that is capable of doing this in nature and, so far, no artificially made system either. To make O_2, PSII uses four photons of wavelength 680 nm in the overall reaction

$$2\text{H}_2\text{O} + 4h\nu \rightarrow 4\text{H}^+ + 4\text{e}^- + \text{O}_2 \quad (8)$$

Despite decades of experimental studies, there are still large uncertainties concerning the detailed chemical steps of the water oxidizing reactions. In light of its fundamental importance in nature, this is therefore one of the most challenging problems in chemistry today.[53−56] A major problem in this context is that the X-ray structure of the enzyme has not yet been obtained. Another problem is that the chemistry of these steps is so unique that it is very hard to find laboratory model reactions with any high degree of similarity to water oxidation. However, although the structure of the water oxidizing complex is not known, sufficient information from EXAFS is available to start model calculations. It is known that the WOC contains four manganese atoms and probably also a calcium and a chlorine atom. The role of calcium is essential, while the role of chloride is less clear. In fact, there are experiments indicating that chloride can be removed with only a minor loss of efficiency.[57] From saturating flash experiments, water oxidation is known to occur in four steps.[58] The intermediates of these steps are denoted S_0 through S_4, and O_2 formation occurs in S_4. The resting dark state of the enzyme is the S_1 state. In each step a photon is adsorbed by a chlorophyll leading to a charge separation, which eventually leads to an oxidation of the WOC. Apart from the electron leaving the WOC cluster upon each oxidation, a proton usually leaves the complex also, see further below.

Different aspects of water oxidation in PSII have been studied by B3LYP calculations. One study[20] was performed to test the hypothesis[54] that one role of the tyrosine residue, which experimentally has been found to appear as a tyrosyl radical in each S state, is to abstract hydrogen atoms from the water and hydroxyl ligands of the manganese cluster. The calculations showed that this mechanism is energetically feasible; the O−H bond strengths of water and hydroxyl coordinated to manganese are about the same as the one in tyrosine. In another study, the

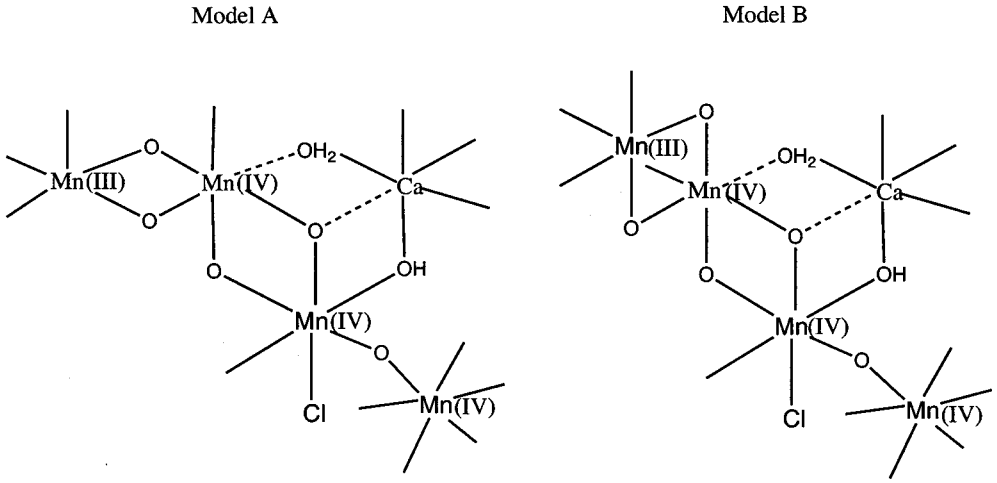

Figure 3. Two different Mn_3 models for the S_2 state of the water oxidizing complex in PSII.

entire reaction sequence for O_2 formation was studied using a model complex containing only one manganese center.[21] A calcium and a chloride was also present in the model complex. Some general principles for these types of redox reactions were proposed and tested. The most important conclusion drawn was that in a typical weak ligand-field redox reaction, in which at least one metal atom changes oxidation state, the position of the excited states before and after the reaction are critical. Either the excited state of the reactant corresponding to the product ground state or the excited state of the product corresponding to the reactant ground state has to be low lying. In the case of water oxidation, this leads to the prediction that an oxygen radical is formed in S_3 prior to O_2 formation. No oxidation of manganese should therefore occur going from S_2 to S_3. Other proposals were that only one manganese center should be redox-active, at least in the critical S_1-S_3 states, and that the role of calcium is to provide chelating energy for reaching the oxygen radical state in S_3. In another recent study also relating to PSII, the cleavage of the O−O bond in a peroxy-bridged manganese dimer was studied using DFT.[59] The possibility to couple the manganese spins ferromagnetically, as opposed to the ground-state antiferromagnetic coupling, was suggested to be important for the mechanism.

Since most of the previous theoretical work on PSII has been recently reviewed,[7] this review will instead briefly describe the most recent, yet unpublished, work on this system. The next step, after the previous proposal of the reaction sequence for O_2 formation,[21] is to put this mechanism into a context of a more realistic manganese cluster since in the previous study only one manganese center was used. One goal with such a study is to investigate if a mechanism where only one manganese atom is redox active is consistent with the fact that a cluster with four manganese atoms was chosen by nature and also to try to understand why this choice was made. Another goal is to identify the main ligand effects that have to be present in the cluster to make the creation of the oxygen radical possible. An actual theoretical determination of the cluster structure and geometry before an X-ray structure has been obtained is probably not realistic but is thought-provoking and

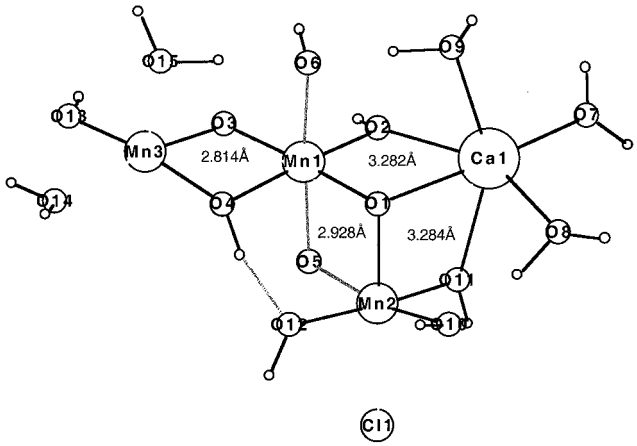

Figure 4. Mn_3 model for the S_3 state of the water oxidizing complex in PSII. Mn1 and Mn2 are Mn(IV) states, Mn3 is a Mn(III) state, and O5 is a radical with a spin population of 0.9.

may be a possibility a decade from now. The key information on which a theoretical manganese cluster model should be built is the EXAFS structural information,[53] but also other results such as those from EPR are very useful for reducing the number of possible structures. After the initial study on the single-center manganese complex, built on about 150 optimized structures, another 150 structures containing two manganese centers were optimized. From these studies general effects of the choice of oxidation states and ligands were thoroughly investigated. One major conclusion drawn from these initial calculations is that too much energy appears to be required to create *terminal* manganese−oxo groups, and such groups are therefore considered as unlikely intermediates. The most recent 150 structures investigated have three manganese centers, and two different types of models were used, see Figure 3 showing possible S_2 structures. A geometry optimized structure of model A-type for the S_3 state is shown in Figure 4. Models A and B are set up in the following way. EXAFS strongly indicates two sets of bis-μ-oxo-bridged manganese centers in which the μ-oxo groups are unprotonated in S_1 and S_2.[53] In that paper the favored suggestion has two *loosely* coupled manganese dimers, but other possibilities were also mentioned. The specific types of Mn_3 models shown in

Figure 3 were selected based on both the preliminary DFT studies and on EPR spectra which indicate strong coupling of at least three manganese centers, in contrast to the suggestion of two loosely coupled dimers. The position of the calcium in the models in Figure 3 is based on recent strontium EXAFS, which indicates two Mn−Sr distances of about 3.5 Å in S_1.[60] Strontium is the only metal that can replace calcium with just a minor loss of activity, and it is assumed that strontium therefore takes the same position as calcium. The clusters in Figure 3 have a central cubic part, where one corner of the cube is missing, The essential chemistry for O_2 formation is suggested to occur on and in this cube. The oxidation states chosen were based on XANES and EPR studies,[53] which show that two Mn(III) and two Mn(IV) are likely oxidation states in S_1 and that there is probably one Mn(II) oxidation state in S_0. The bottom terminal manganese in Figure 3 appears at the moment to be the most likely redox-active center, corresponding to the one discussed in the previous study. Different Mn_3 structures were then obtained mainly by switching ligands around, which essentially comes down to moving hydrogen atoms between the water and hydroxyl ligands.

The main criterion for choosing a proper model for O_2 formation is based on the fact that about 90 kcal/mol is available for performing the desired chemistry in each S-state transition. This value comes from the O−H bond strength in tyrosine, which is about 87 kcal/mol. As mentioned above, the tyrosine appears as a neutral radical in the beginning of each S state and returns to its normal nonradical form at the end of each S state. This energy is used to remove an electron from manganese and a proton from a water (or hydroxy) ligand. There are two leading proposals as to the details of this process. In the first one,[54] the tyrosyl radical abstracts a hydrogen atom from a water ligand. In the second,[56] the tyrosyl radical only abstracts an electron from manganese while the proton on the water ligand is abstracted by a base. Independent of which detailed mechanism is correct, the energetic criterion of about 90 kcal/mol available in each S state remains the same, provided that the charge of the cluster remains the same. It should be added that with the second mechanism there is also the possibility that the charge of the cluster changes, which has to be investigated using slightly different criteria. The energetic criterion, which amounts to removing an electron and a proton from the cluster to see if this requires about 90 kcal/mol, turns out to be extremely selective, and only very few structures pass this test.

The investigation of possible structures is in progress, but a few preliminary results can still be reported at this stage. As in the previous study on a complex with a single manganese center, the oxygen radical appearing in S_3 is created by removing a hydrogen atom from a water (O2 in Figure 4) that is bridging between manganese and calcium. This leads to a substantial reduction of the Mn1−Ca distance, which gives sufficient additional energy to barely reach the oxygen radical state. Independent of model used, model A or B, the oxygen radical always appears at O5. To reach this oxygen radical, the trans effects are very important and sometimes extremely sensitive to the choice of ligands. Two examples of this sensitivity will be mentioned here. First, the trans position at O10 is very critical, and with a water ligand at this position, the oxygen radical state is too high by 10 kcal/mol in some models. This is equivalent to saying that the O−H bond strength of the water at O2 is increased by 10 kcal/mol if O10 is additionally protonated, which is quite remarkable since they are at different ends of the cluster. The second trans effect to be mentioned here is the one at O4. This μ-oxo group becomes protonated from O12 as the O2 hydrogen is removed, which leads to an increase of the Mn1−Mn3 distance. The reason is that this releases some of the strong μ-oxo trans effect. The second Mn−Mn distance (Mn1−Mn2) is also increased because O5 becomes a radical. This leads to the surprising effect noted in the EXAFS data that *both* short Mn−Mn distances are increased in the S_2-S_3 transition. It should be added in this context that the calculated Mn−Mn distances using the present rather small basis sets are 0.05−0.1 Å too long. As in the previous study, the O−O bond could finally be formed by an external attack from a water molecule on the oxygen radical at the O5 position, leading to a bridging O_2H ligand. This means that the two oxygens forming O_2 should have different chemical origins and should exchange with different rates with solvent water, which is in accordance with isotope labeling experiments.[61] Other mechanisms for O−O bond formation are presently under investigation. Probably the most important property of the Mn_3 cluster compared to the previous single manganese complex is that the radical oxygen is well protected against internal proton transfers in S_3 and the same oxygen is reasonably well protected in S_2. In the previous small model, this oxygen is a terminal oxo ligand with a very large proton affinity in S_2 and it was difficult to understand why it should not be protonated from the Mn−Ca bridging water ligand, which would destroy the possibility to form the oxygen radical. This was actually noted as a major problem in the previous study. In the Mn_3 cluster, this oxygen is a μ-oxo bridge between two Mn(IV) centers in S_2, and this type of bridge is known not to be easily protonated and is therefore much less likely to take a proton from the water ligand. One interesting question remaining is, of course, where the fourth manganese center should be, but at present there is not sufficiently critical information available to make any speculation of this meaningful. To agree with the EXAFS information, it could, for example, be placed with a single μ-oxo bridge to Mn2, which should lead to an Mn−Mn distance of about 3.3 Å.

C. Other Mechanisms

1. Nitrogenases

Nitrogenases are enzymes that catalyze the reduction of N_2 to ammonia. Three types of these enzymes contain different inorganic constituents: one containing Mo, Fe, and S^{2-}, one containing V, Fe, and S^{2-}, and finally one with Fe and S^{2-} alone. The mechanisms of these enzymes have recently been re-

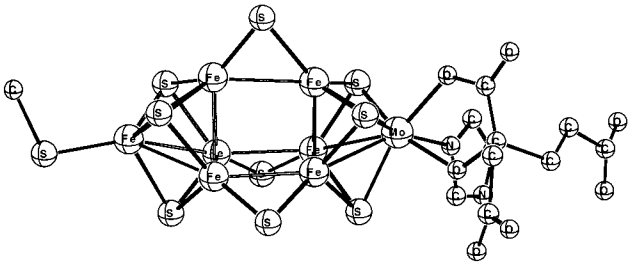

Figure 5. X-ray structure of the FeMo cofactor from *A. Vinelandii.*

viewed.[62−64] A major breakthrough in this area occurred some years ago when the X-ray structures of both component proteins of the molybdenum-containing nitrogenase were solved.[65−67] The FeMo cofactor was shown by this work to be composed of one molybdenum and seven iron atoms arranged in two incomplete M_4 S_3 cubanes, each one with a missing sulfur. The two cubanes are linked by three sulfur bridges, see Figure 5. All but one of the irons are three-coordinate, while molybdenum is six-coordinate. Under optimal conditions, the overall stoichiometry of dinitrogen reduction by the molybdenum nitrogenase can be written

$$N_2 + 8H^+ + 8e^- + 16ATP \rightarrow 2NH_3 + H_2 + 16ADP + 16P_i \quad (9)$$

N_2 becomes bound at the FeMo cofactor in the MoFe protein. The electrons are taken from the Fe−protein in a process where ATP is consumed, two for each electron, with an electron-transfer path that passes over an Fe_8S_8 cofactor (P cluster). The protons are delivered from the medium surrounding the FeMo cofactor in a process that is probably strongly coupled to the electron transfer. It can be noted from reaction 9 that when ammonia is formed it is unavoidable that one hydrogen molecule is formed for the molybdenum-containing nitrogenase. In the vanadium-containing nitrogenase, three hydrogen molecules are formed for each nitrogen molecule consumed. Due to the complexity of reaction 9 and of the FeMo cofactor, the investigation of these processes by theoretical methods has to be approached in steps initially using quite simple models. In an early study, the binding of N_2 was studied using some iron monomer models at the MP2 level and for some larger models at the UHF level.[68] N_2 was found to be loosely bound in most cases with the triple bond retained, while a few examples were found where N_2 is activated and has a longer N−N bond. It was suggested that a dimer site of Fe(III) centers with low coordination number might be useful for catalysis of N_2 reduction. In a first attempt to study the mechanism of the N_2 reaction by DFT methods, all the steps of ammonia formation from N_2 were investigated using a simple Fe_2 model of the FeMo cofactor.[69] The main result of that study is that some Fe(I) character appears to be required for the cluster to perform the most difficult first step of reaction 9, where N_2H is formed. Fe(I) character is achieved by starting with a cluster with mainly Fe(II) atoms and then binding hydrogen atoms to the sulfurs bridging the irons. Another major point of that study is that since the ammonia formation occurs in essentially decoupled steps with the same driving force, a mechanism has to be found in which a hydrogen atom (proton plus electron) binds to the cluster, either to N_2 or to sulfur, with the same energy in each step. From the heat of formation of ammonia, this energy can be estimated to be about 50 kcal/mol. If the binding energy is significantly smaller than this value, the step would be endothermic and not occur, and if the binding energy is much higher, energy would be wasted. A mechanism was suggested where this requirement was fulfilled in each step. Some of the most critical steps were finally tested on larger clusters with up to eight iron atoms. In another study, essentially the same mechanism was tested on a cluster containing all seven irons and molybdenum, using periodic boundary conditions.[70] It was shown that initially three hydrogen atoms have to be bound on the cluster before N_2 is reduced, in perfect agreement with the experimental result that three electrons need to be transferred to the FeMo cofactor to start the reaction.[63] In still another set of theoretical studies, different positions where N_2 might bind to the cluster were compared using the full FeMo cofactor as a model with all its ligands.[71] The geometry obtained for the bare cluster using a nonhybrid DFT method is in impressively good agreement with the experimental X-ray structure, with deviations on the bond distances of typically less than 0.05 Å. The optimal geometry found for N_2 was asymmetric between the two incomplete cubane clusters of the cofactor. A transition state for ammonia formation was postulated in which one of the nitrogens is fully protonated while the other one is unprotonated. On energy minimization, the N−N bond broke and the process was found to be exothermic by several tens of kcal/mol. A reaction coordinate for formation of H_2 was also determined.

2. Hydrogenases

Hydrogenases are enzymes that catalyze the reversible oxidation of molecular hydrogen ($H_2 \rightleftharpoons 2H^+ + 2e^-$). The products formed in the H_2 activation can be used by bacteria for reduction of inorganic molecules such as CO_2, SO_4^{2-}, NO_3^-, and O_2. For hydrogenases located on the bacterial membrane, a transmembrane proton gradient can be created which leads to ATP formation. In that way, many microorganisms can use hydrogen gas as a source of energy. The majority of hydrogenases contain iron atoms arranged in Fe−S clusters, and many of them also contain one nickel atom in the active site. The nickel-containing enzymes are termed Ni−Fe hydrogenases. On the basis of an X-ray structure[72] and spectroscopic IR studies,[73] the active site for H_2 activation was identified as a bimetallic Fe−Ni complex where iron has two CN and one CO ligand, which is an unprecedented ligand set in biochemistry. On the basis of experimental work, several mechanisms have been proposed for the Ni−Fe hydrogenase over the years. Recently, the first quantum chemical studies on this system were carried out.[74,75] The mechanism for H_2 activation found is shown in Figure 6. The only type of complex found to activate H_2 has an odd number of electrons and should thus be EPR visible. To model

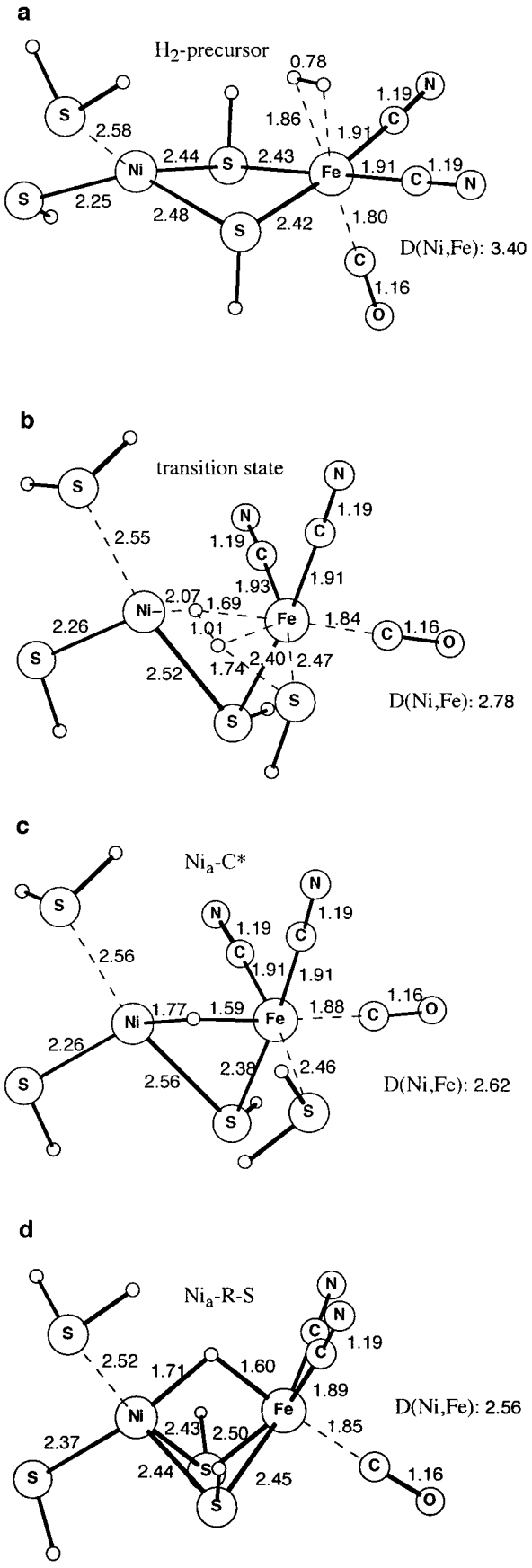

Figure 6. Mechanism for the activation of H_2 by Ni−Fe hydrogenase.

this with a neutral complex requires one of the terminal cysteines to be modeled as protonated, as shown in Figure 6. The alternative is to have a negatively charged complex and all cysteines modeled as SH^-, but this leads to substantially worse agreement with experiments for the rate of the H_2 reaction. The activation reaction starts with the hydrogen first becoming molecularly bound to iron, see Figure 6a. This gives a rationale for the unusual choice of ligands on iron, since these strong-field ligands force iron into a low-spin configuration, which is favorable for molecular precursor binding. No corresponding minimum on the nickel side was found. In the next step there is a heterolytic splitting of H_2 going over a transition state, as shown in Figure 6b. The proton initially becomes bound to a bridging cysteine while the hydride eventually becomes bound between iron and nickel. The bridging hydride forces the metals closer together and explains the short distance observed in the recent X-ray structure of the reduced enzyme, Ni_a−R−S in Figure 6d.[76] Ni_a−R−S differs from the product of the H_2 splitting, Ni_a−C* in Figure 6c, by one proton and one electron that has left the complex. It should be added that the heterolytic splitting of H_2 found in these studies logically sets up the system for moving the electrons and protons in different directions along separate pathways from the complex, as is known to occur in the enzyme. In a recent DFT study,[77] calculations on a series of known FeCO complexes were used to calibrate the calculated CO bond distances with measured IR stretching frequencies. Using this calibration curve, the calculated CO bond distances for different states of a nickel−iron hydrogenase active-site model could be assigned to corresponding IR frequences. By comparing these IR frequencies to the experimental spectra obtained for different intermediates of the nickel−hydrogenase enzyme, these intermediates could be putatively characterized.

3. Cytochrome P450

Several heme−proteins reduce oxygen in a similar fashion as CcO (see section III.A), and they have also been studied by quantum chemical methods. The detoxification enzyme cytochrome P450 is in fact very similar to CcO in the O_2 activation steps. One difference between CcO and P450 is the axial ligand on the iron center being a protonated histidine in CcO and a cysteine in P450. O_2 coordinates to the reduced Fe(II) form of both enzymes, which in the P450 case has a negatively charged axial ligand, while the corresponding form of CcO has a neutral axial ligand. To form a peroxide state, in CcO an electron is received from the Cu_B center while in P450, where such a copper center does not exist, the second electron is introduced via a flavin-containing electron-transport chain. Starting then from very similar (porf)Fe(III)−O−OH intermediates, the O−O bond is broken without the introduction of further electrons to the active site in both CcO and P450. In P450 it has been believed that a radical is formed at the porphyrin ring in the O−O splitting reaction step, but a few researchers have suggested the formation of a sulfur radical in thiolate−heme proteins. Recent DFT calculations on models of thiolate−heme compound I support the existence of a sulfur radical on this species.[78,79] The electronic structure of other intermediates of the cytochrome P450 reactions has

also been explored by DFT methods.[78,80−82] DFT calculations have also been used to investigate the interaction between models of P450 and various substrate molecules.[33]

The O−O activation in P450 has been studied at the DFT level (using the BPW91 functional).[78,80] A very different approach was used compared to the one described above for CcO. Completely free electrons and protons were introduced into the reaction center, and extremely exothermic (several hundreds of kcal/mol) reaction steps with no activation barrier for the formation of compound I, (porf)Fe(IV)=O, and water were therefore obtained. The large exothermicity obtained for these reaction steps strongly violates the thermoneutrality criterion for biological reactions discussed in section III.A above, and the value of this type of modeling is therefore questionable. Calculations on P450 are reviewed in a separate article in this volume, which is referred to for further details.[84]

4. Heme Peroxidases

There are also large similarities between CcO and P450 on one hand and heme peroxidases and catalases on the other. The peroxidases and catalases activate the O−O bond in H_2O_2, and in fact, this substrate can also be used for both CcO and P450 but starting from the oxidized Fe(III) form. In a recent density functional study of the formation of compound I, (porf)Fe(IV)=O, in heme peroxidases[85] (CCP, HRP, APX, etc.) a model similar to the one described above for the iron part of CcO was used. In a first step, after the hydrogen peroxide has coordinated to the iron center, a distal histidine is abstracting a proton from the peroxide and the same (porf)Fe(III)−O−OH intermediate as in CcO is formed. To retain the oxidation state of iron in this step, the proximal histidine ligand is altered from imidazolate to imidazole. The next step, breaking the O−O bond and forming the oxoferryl intermediate compound I, (porf)Fe(IV)=O, and water, is very similar to the one that occurs in CcO and P450. The transition state for this step in a model of a heme−peroxidase is shown in Figure 7. In most peroxidases it is believed that a radical is formed on the porphyrin ring in this step. In the density functional study (B3LYP) of the O−O splitting step in peroxidase,[85] a barrier of 10 kcal/mol was calculated, involving a spin crossing. Models of peroxidase compounds I and II have also been studied using the BP86 density functional together with the broken symmetry formalism.[86] The detailed nature of the ground state of compound I, determined by the character of the porphyrin radical, was discussed on the basis of those calculations. The electronic properties of compounds I and II were also investigated in another DFT study,[87] where Fe−O stretching frequencies were also calculated for different species and compared to experimental results. Models of compounds I and II were also studied in ref 82 where, in particular, the effects of the proximal ligand were discussed and comparisons were made between cytochrome P450 and peroxidase. In ref 88, saddle distortions in models of peroxidase compound I were discussed on the basis of DFT calculations. The mechanisms of peroxidase activation have also

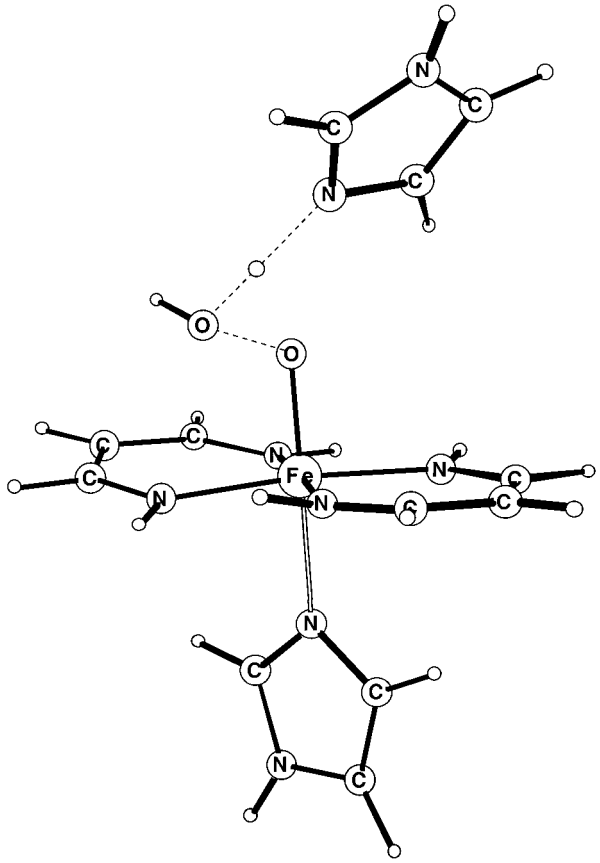

Figure 7. The transition state for activating O_2 in a model for a heme peroxidase.

been investigated using different naked metal cations as models for the heme group.[89] The methods used in the calculations on these small model systems were second-order perturbation theory and coupled-cluster theory. The main conclusion in that study was that a distal proton acceptor (modeled by a water molecule) drastically decreases the barrier for the HOOH to H_2OO isomerization. Several DFT studies on models of other heme-containing enzymes have also been made, e.g., refs 90−93, of which some were discussed in the recent review.[7]

5. Non-Heme Oxygenases

Theoretical studies of the mechanisms for O_2 activation by tyrosinase and hemocyanin, which contain a bimetallic copper center, and by methane monooxygenase (MMO), which contain a bimetallic iron center, have recently been reviewed.[7] A very similar metal center is also found in ribonucleotide reductase (RNR). The present indications are that the O_2 splitting mechanism is rather different in these enzymes as compared to the heme-containing enzymes discussed above. In the latter systems, the splitting of the O−O bond occurs for O−OH or even $O-OH_2^+$, while no proton seems to be involved in the former systems. For MMO and RNR, B3LYP calculations using an iron dimer model including all first-sphere ligands suggest that the splitting of O_2 occurs by an initial formation of a rather symmetric Fe−O_2−Fe peroxide structure (compound **P**), for which O_2 splits and the oxygens move to bridging μ-oxo positions, compound **Q** in MMO and compound **X** in

RNR.[19] A barrier in reasonable agreement with experiment was obtained using B3LYP. The mechanism for activating methane was also investigated in the same study, and a direct hydrogen abstraction mechanism was found. In another study an unsaturated charged iron complex was used as a model for the iron dimer.[15,16] The charge in this model leads to a very strongly bound methane molecule which in turn leads to a C−H activation mechanism with a four-centered transition state. These results were also reviewed recently. A DFT study has also been done on the electronic structure of a laboratory model complex with two Fe(III) and bridging μ-oxo bonds.[94] For tyrosinase and hemocyanin, calculations indicate a similar mechanism as that for MMO and RNR for the O_2 activation.[8−12] However, the use of ammonia ligands for the actual histidines in some of these studies make direct conclusions concerning the mechanism in the enzymes somewhat questionable. In fact, more recent studies using imidazole models suggest that O_2 may never split in a separate first step in the enzymes. In contrast, for some experimental model systems with highly strained multidentate ligands, which is quite different from the situation in the enzyme, there is little doubt that O_2 actually splits without being protonated.[10,12]

6. Molybdenum Oxotransferases

The molybdenum-containing oxotransferase enzymes catalyze oxygen-atom transfer to or from biological substrates in the nitrogen, sulfur, and carbon cycles. For a model dioxo−molybdenum complex, a catalytic cycle has been set up for this type of reaction using correlated ab initio methods (third-order Møller−Plesset perturbation theory).[95] The oxygen transfer step to the substrate PMe_3 is found to occur with a barrier of 14 kcal/mol to form an intermediate which is extremely stable by 69 kcal/mol compared to the reactants. This stability is partly explained by the formation of a formal Mo−O triple bond. The displacement of the $OPMe_3$ product by water occurs over a barrier of 19 kcal/mol. The reaction between a Mo(IV) and Mo(VI) then generates Mn(V) in a process which is exothermic by 14 kcal/mol, and O_2 finally oxidizes Mn(V) to Mn(VI) to complete the cycle. In another study on models of these enzymes, both extended Hückel and DFT calculations were used to set up a reaction sequence.[96] A direct attack of hydrogen sulfite on an oxo ligand is found to be a favorable pathway. No effect of a formal Mn−O triple bond formation was found for the model system used, in contrast to the case mentioned above.

7. Iron–Sulfur Proteins

Iron−sulfur proteins are often electron-transfer agents, and it is therefore important to understand how the electronic structure features of iron−sulfur complexes determine the wide range of redox potentials for these systems. Also, the interaction with the protein environment is expected to play an important role in determining the redox properties of iron−sulfur clusters. Density functional calculations on this subject have been reported for synthetic 1Fe, 2Fe, and 4Fe iron−sulfur complexes in solution.[97] From broken symmetry and high-spin state calculations, the Heisenberg parameter J could be determined, as well as the energies of the low-spin ground states (see further section IV.B). Environmental effects were modeled through a continuum dielectric to calculate the solvent contribution to the redox potentials. A good correlation was found between predicted and measured redox potentials. In a more recent study,[98] the redox potentials of [2Fe2S] clusters in the two proteins ferredoxin and phthalate dioxygenase reductase (PDR) were calculated using density functional theory and the Heisenberg Hamiltonian formalism. The effects from the protein environment were obtained from a finite-difference solution to the Poisson−Boltzmann equation. The calculated redox potentials, −1.007 and −0.812 V for ferredoxin and PDR, respectively, deviate significantly from the experimental values of −0.440 and −0.174 V while the experimental trend is well reproduced.

8. Superoxide Dismutases

Manganese, iron, and copper−zinc superoxide dismutases (SODs) are important detoxifying agents for the superoxide radical anion. In two recent papers,[99,100] redox potentials were calculated for manganese and copper−zinc SOD enzymes using density functional theory in combination with different levels of electrostatic descriptions of the protein environment. For the MnSOD enzyme it was shown that second-shell ligands on the manganese center had to be included in the quantum mechanical part of the model to obtain good agreement with the experimental redox potential.[99] It was also shown that the simple electrostatic continuum model gave almost the same results as the more complicated model including the entire protein, in particular for the larger quantum mechanical models. Similarly, for the CuZn-SOD enzyme it was shown that the calculated redox potential only differed by 3 kcal/mol between a dielectric continuum model ($\epsilon = 4$) and a full protein treatment.[100] Mechanistic aspects of electron- and proton-transfer reaction steps were discussed on the basis of calculated redox potentials and pK_a values.

IV. Spectroscopic Applications

Spectroscopy is the experimentalists tool to investigate nature since only energy differences can be obtained experimentally. Quantum chemistry has the great advantage that total energies can be obtained, and the chemical problems can therefore be studied more directly. However, in biochemistry the chemical problems are often so complicated that progress can only be achieved by an intimate cooperation between theory and experiment. This can be done both by obtaining complementary information from theory, which is not available from experiments, but also by direct interpretations of experiment by theoretical calculations. In this section the present status of calculation of spectra for biological transition-metal complexes will be briefly described, with examples both from ab initio and DFT studies.

A. Electronic Spectra

One of the first applications of the CASPT2 method on biochemical transition-metal complexes was per-

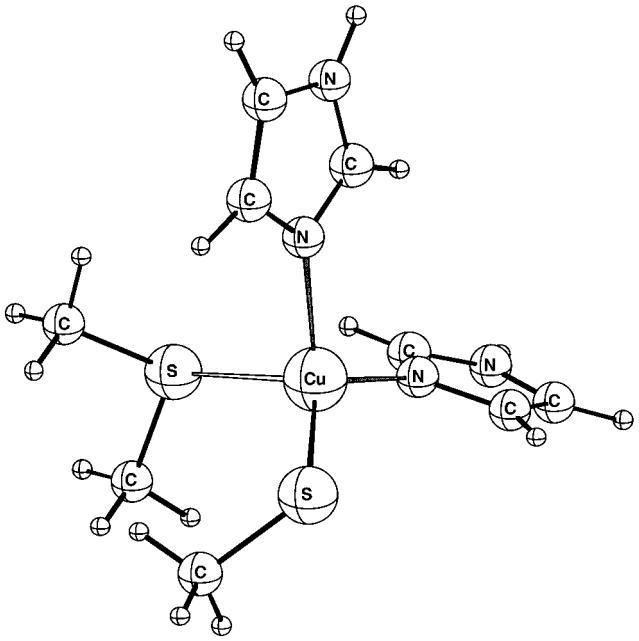

Figure 8. Optimized structure of the blue copper protein complex.

formed for plastocyanin.[14,101] This is a four-coordinated $Cu(His)_2(Cys)(Met)^+$ complex which plays an important role in photosynthesis as an electron-transfer complex. The optical spectrum of this complex had been studied earlier using the X_α method.[102] Several chemical models were used for this complex in the CASPT2 study, but the smallest model that gave a consistent description of the spectrum was Cu(imidazole)$_2$(SCH$_3$)(S(CH$_3$)$_2$)$^+$, see Figure 8. Neither modeling the histidines by ammonia nor the cysteine by SH^- or the methionine by SH_2 gave an accurate enough description of the spectrum. Thirteen electrons were correlated in an active space of 12 orbitals using a basis set of DZP quality for Cu and S and DZ quality for C, N, H. The six lowest electronic transitions were assigned with an error of less than 2000 cm^{-1} (5 kcal/mol). Calculations performed for the closely related protein complexes of stellacyanin[103] and of axial[101] and rhombic type 1 copper proteins,[104] gave a similar accuracy compared to experiments. The type of proteins which contain these copper complexes are called blue copper proteins, and in the case of plastocyanin, the bright blue color originates from an electron transfer from a Cu 3d$-S_{Cys}$ bonding to a singly occupied antibonding orbital of the same character, with an excitation energy of 16 700 cm^{-1}. Altogether, eight lines were assigned for plastocyanin. The most problematic line to assign was an excitation to an e^2A' state at 23 440 cm^{-1} which was calculated at 31 264 cm^{-1}. It is notable that the assignment of the calculated line was not at all to the experimental line which was closest in energy, which is at 32 500 cm^{-1}. Instead, trends obtained for smaller chemical models of the errors due to basis set and geometry deficiencies were used to make the final assignment. Another uncertainty is the effect of the protein environment. This shows that the assignment of an electronic spectrum based on theoretical results is far from trivial. The theoretical result will depend on the correlation treatment (CASPT2), the basis set, the model used for the active site, and the structure. On top of this, the experiment also has inherent uncertainties. The bands are broad and overlapping and a Gaussian resolution is based on assumptions about the number of bands and is often not unique. It is not certain that all bands are of electronic origin, the sample may not be pure, etc. In the case of plastocyanin, one of the bands was for these reasons left unassigned. This band was not found in model compounds nor in the closely related nitrite reductase.

An interesting aspect of all studies of biochemical systems is the question of the influence of the protein, see also section II.B. In the study of the blue copper proteins, the spectra were calculated with and without models of the surrounding protein. The calculations were performed on Cu(imidazole)$_2$(SH)(SH$_2$)$^+$ using the respective crystal geometries of the three proteins, plastocyanin, cucumber basic protein, and nitrite reductase. A point-charge model of the surrounding protein and solvent molecules was used.[105] The calculations show that the surrounding cannot be neglected with effects of up to 2500 cm^{-1}. It was also shown that in order to reproduce the qualitative trends between plastocyanin and nitrite reductase, some critical bonds had to be optimized at the CASPT2 level. The experimental X-ray structures are not accurate enough for reproducing these sensitive trends.

B. Spin–Spin Spectra

Since spin coupling does not appear explicitly in DFT, the calculation of those states that require a multideterminental description represents a fundamental problem for DFT methods. This problem is particularly evident for optical spectra since normally most excited states observed experimentally are multideterminental spin states. In contrast, the calculation of the excitation energy from a closed-shell ground state to the lowest excited triplet state represents no problem. There are two different ways to still obtain reasonable information about the positions of the multideterminental spin states. In one of these approaches the excitation energies are obtained by response theory.[106] This type of method is at the moment only available for closed-shell ground-state systems, which means that it is not applicable for most transition-metal complexes in biochemistry. For organic systems the experience is that the method gives quite accurate excitation energies unless charge-transfer states are considered.[107] The second way to obtain information about multideterminental spin states is to use the broken symmetry/spin projection method, which has recently been reviewed.[108] This approach can be applied for two (or more) weakly interacting spin centers. The interaction between two centers with spin vectors $\mathbf{S}_A$ and $\mathbf{S}_B$, respectively, can be described by the Heisenberg Hamiltonian,

$$H_{spin} = J\mathbf{S}_A\mathbf{S}_B \qquad (10)$$

The successive spin states of the Heisenberg ladder are given by the Landé interval rule, $E(S_t) - E(S_t$

$-1) = JS_t$, where S_t is the total spin, ranging from $S_A + S_B$ to $|S_A - S_B|$, where S_A and S_B are the spin quantum numbers of the two centers. The Heisenberg J parameter can be determined from the energy difference between the highest spin state (HS), with aligned spin vectors for the two centers, and a broken symmetry state (BS), with oppositely aligned spin vectors on the two centers, using the formula

$$E_{HS} - E_{BS} = 2JS_AS_B$$

Both the energy of the high-spin state, E_{HS}, and the energy of the broken symmetry state, E_{BS}, can be obtained from spin-unrestricted density functional calculations. However, it should be noted that it is not trivial to obtain SCF convergence to a low-spin broken symmetry wave function, which should have internal high-spin coupling on each center and low-spin coupling between the two centers. When the J parameter is determined, the energy of all the different spin states can be calculated from the Landé interval rule given above.

The Heisenberg Hamiltonian formalism has, for example been applied to a set of five manganese−oxo dimer complexes.[109] Those manganese−oxo dimer complexes, which have been synthesized and structurally characterized by X-ray diffraction, were studied as models for the water oxidizing complex in photosystem II (see also section III.B). One of the main goals of that study was to calculate the Heisenberg coupling parameters for the different complexes and compare them with the corresponding experimental values, based on magnetic susceptibility measurements. The experimental results for the set of Mn−oxo complexes range from weakly ferromagnetic coupling to strongly antiferromagnetic coupling, and despite the quantitative deficiencies in the calculated values, the experimental trend was well reproduced. The electronic structures of these synthetic dinuclear manganese−oxo complexes were explored to gain insight into the ease of multielectron transfer and coupled proton transfer in the related water oxidizing complex.[109]

An alternative to the broken symmetry formalism is the valence-bond configuration-interaction method for calculating and analyzing excited-state antiferromagnetism and ground-state spin coupling based on high-spin state derived matrix elements.[110] A mixture of density functional calculations and experimental spectra have been used to evaluate the strength of excited-state antiferromagnetism in oxo-bridged iron dinuclear complexes and peroxo-bridged copper dinuclear complexes.[110−112]

V. Conclusions

Accurate quantum chemical treatments of transition-metal complexes in biochemical systems is a relatively new area. In the present review, a description of the current status of these treatments has been made. This description has focused on a few examples under current investigation to illustrate the different aspects that enter studies of this type. There are at least two striking differences in the applications on these systems as compared to other transition-metal complexes, for example, in the area of homogeneous catalysis where there is much more experience of using quantum chemical methods. One notable difference is that the overall chemistry that the biochemical complexes are involved in is considerably more complicated than in a typical catalytical cycle of a laboratory process. A second striking difference is that the amount of experimental information, at least for the enzymes discussed in detail in this review, is immense. There are often decades of experimental investigations done by researchers who have spent a large part of their careers on one particular enzyme. This means that even though point contributions in this area are being and will be made, in the long run quantum chemistry will probably become more involved in the overall understanding of the mechanisms of the enzymes. To make significant contributions, the large amount of biochemical information will have to be put in the context of a quantum chemical modeling, which is not a trivial matter. In this review, two examples from two important enzymes, CcO and PSII, have therefore been described in some detail in order to give the entire context of the calculations. These are both projects that have gone on for a few years and will probably continue for another few years. The review has also tried to cover other areas of accurate quantum chemical treatments of biochemical transition-metal systems. Examples have, for example, been given from some spectroscopic applications and from calculations on magnetic and redox properties. The number of applications is still not large but it can safely be predicted that the area is going to grow rapidly in the future, perhaps to become one of the main areas for accurate quantum chemical studies.

VI. References

(1) Bauschlicher, C. W., Jr.; Siegbahn, P.; Pettersson, L. G. M. *Theor. Chim. Acta* **1988**, *74*, 479−491.
(2) Goodgame, M. M.; Goddard, W. A. *J. Phys. Chem.* **1981**, *85*, 215−217.
(3) Becke, A. D. *Phys. Rev.* **1988**, *A38*, 3098.
(4) Becke, A. D. *J. Chem. Phys.* **1992**, *96*, 2155−2160.
(5) Becke A. D. *J. Chem. Phys.* **1993**, *98*, 5648−5652.
(6) Friesner, R. A.; Beachy, M. D. *Curr. Opin. Struct. Biol.* **1998**, *8*, 257−262.
(7) Siegbahn, P. E. M.; Blomberg, M. R. A. *Annu. Rev. Phys. Chem.* **1999**, *50*, 221−249.
(8) Bernardi, F.; Bottoni, A.; Casadio, R.; Fariselli, P.; Rigo, A. *Int. J. Quantum Chem.* **1996**, *58*, 109−119. Bernardi, F.; Bottoni, A.; Casadio, R.; Fariselli, P.; Rigo, A. *Inorg. Chem.* **1996**, *35*, 5207−5212.
(9) Mahapatra, S.; Halfen, J. A.; Wilkinson, E. C.; Pan, G.; Wang, X.; Young, V. G., Jr.; Cramer, C. J.; Que, L., Jr.; Tolman, W. B. *J. Am. Chem. Soc.* **1996**, *118*, 11555. Cramer, C. J.; Smith, B. A.; Tolman, W. B. *J. Am. Chem. Soc.* **1996**, *118*, 11283.
(10) Flock, M.; Pierloot, K. *J. Phys. Chem. A* **1999**, *103*, 95−102.
(11) Lind, T.; Siegbahn, P. E. M.; Crabtree, R. H. *J. Phys. Chem.* **1999**, *103*, 1193−1202.
(12) Bérces, A. *Inorg. Chem.* **1997**, *36*, 4831−4837.
(13) Ryde, U.; Olsson, M. H. M.; Roos, B. O.; Pierloot, K. *J. Mol. Biol.* **1996**, *261*, 586−596.
(14) Ryde, U.; Olsson, M. H. M.; Roos, B. O.; Pierloot, K.; De Kerpel, J. O. A. *Encycl. Comput. Chem.* **1998**, *3*, 2255−7270.
(15) Yoshizawa, K.; Shiota, Y.; Yamabe, T. *Organometallics* **1998**, *17*, 2825−2831.
(16) Yoshizawa, K.; Ohta, T.; Shiota, Y.; Yamabe, T. *Chem. Lett.* **1997**, 1213−1214; *ibid. Bull. Chem. Soc. Jpn.* **1998**, *71*, 1899.
(17) Siegbahn, P. E. M.; Crabtree, R. H. *J. Am. Chem. Soc.* **1997**, *119*, 3103−3113.
(18) Siegbahn, P. E. M.; Crabtree, R. H.; Nordlund, P. *J. Biol. Inorg. Chem.* **1998**, *3*, 314−317.
(19) Siegbahn, P. E. M. *Inorg. Chem.* **1999**, *38*, 2880−2889.

(20) Blomberg, M. R. A.; Siegbahn, P. E. M.; Styring, S.; Babcock, G. T.; Åkermark, B.; Korall, P. *J. Am. Chem. Soc.* **1997**, *119*, 8285−8292.
(21) Siegbahn, P. E. M.; Crabtree, R. H. *J. Am. Chem. Soc.* **1999**, *121*, 117−127.
(22) Stevens, P. J.; Devlin F. J.; Chablowski, C. F.; Frisch, M. J. *J. Phys. Chem.* **1994**, *98*, 11623.
(23) Lee, C.; Yang, W.; Parr, R. G. *Phys. Rev.* **1988**, *B37*, 785.
(24) Vosko, S. H.; Wilk, L.; Nusair, M. *Can. J. Phys.* **1980**, *58*, 1200.
(25) (a) Perdew, J. P.; Wang, Y. *Phys. Rev. B* **1992**, *45*, 13244. (b) Perdew, J. P. In *Electronic Structure of Solids*; Ziesche, P., Eischrig, H., Eds.; Akademie Verlag: Berlin, 1991. (c) Perdew, J. P.; Chevary, J. A.; Vosko, S. H.; Jackson, K. A.; Pederson, M. R.; Singh, D. J.; Fiolhais, C. *Phys. Rev. B* **1992**, *46*, 6671.
(26) Curtiss, L. A.; Raghavachari, K.; Trucks, G. W.; Pople, J. A. *J. Chem. Phys.* **1991**, *94*, 7221.
(27) Bauschlicher, C. W., Jr.; Ricca, A.; Partridge, H.; Langhoff, S. R. In *Recent Advances in Density Functional Methods, Part II*; Chong, D. P., Ed.; World Scientific Publishing Co.: Singapore, 1997; p 165.
(28) Armentrout, P. B.; Kickel, B. L. In *Organometallic Ion Chemistry*; Freiser, B. S., Ed.; Kluwer: Dordrecht, 1995; pp 1−45.
(29) Blomberg, M. R. A.; Siegbahn, P. E. M.; Svensson, M. *J. Chem. Phys.* **1996**, *104*, 9546−9554.
(30) Ricca, A.; Bauschlicher, C. W., Jr. *J. Phys. Chem. A* **1997**, *101*, 8949−8955.
(31) Blomberg, M. R. A.; Siegbahn, P. E. M. Unpublished results.
(32) Ricca, A.; Bauschlicher, C. W., Jr. *J. Phys. Chem.* **1994**, *98*, 12899−12903.
(33) Distefano, G. *J. Res. Natl. Bur. Stand. A* **1970**, *74*, 233.
(34) Halle, L. F.; Armentrout, P. B.; Beauchamp, J. L. *Organometallics* **1982**, *1*, 963.
(35) Sunderlin, L. S.; Wang, D.; Squires, R. R. *J. Am. Chem. Soc.* **1992**, *114*, 2788.
(36) Koch, W.; Hertwig, R. H. *Encycl. Comput. Chem.*, in press.
(37) Lewis, K. E.; Golden, D. M.; Smith, G. P. *J. Am. Chem. Soc.* **1984**, *106*, 3905−3912.
(38) Gardner, K. A.; Mayer, J. M. *Science* **1995**, *269*, 1849 and private communication.
(39) Roos, B. O.; Andersson, K.; Fülscher, M. P.; Malmqvist, P.-Å.; Serrano-Andrés, L.; Pierloot, K.; Merchán, M. In *Advances in Chemical Physics: New Methods in Computational Quantum Mechanics*; Prigogine, I., Rice, S. A., Eds.; Wiley: New York, 1996; Vol. XCIII, pp 219−331.
(40) Åqvist, J.; Warshel, A. *Chem. Rev.* **1993**, *93*, 2523−44.
(41) Blomberg, M. R. A.; Siegbahn, P. E. M.; Babcock, G. T. *J. Am. Chem. Soc.* **1998**, *120*, 8812−8824.
(42) Frisch, M. J.; Trucks, G. W.; Schlegel, H. B.; Gill, P. M. W.; Johnson, B. G.; Robb, M. A.; Cheeseman, J. R.; Keith, T.; Petersson, G. A.; Montgomery, J. A.; Raghavachari, K.; Al-Laham, M. A.; Zakrzewski, V. G.; Ortiz, J. V.; Foresman, J. B.; Cioslowski, J.; Stefanov, B. B.; Nanayakkara, A.; Challacombe, M.; Peng, C. Y.; Ayala, P. Y.; Chen, W.; Wong, M. W.; Andres, J. L.; Replogle, E. S.; Gomperts, R.; Martin, R. L.; Fox, D. J.; Binkley, J. S.; Defrees, D. J.; Baker, J.; Stewart, J. P.; Head-Gordon, M.; Gonzalez, C.; Pople, J. A. *Gaussian 94 Revision B.2*; Gaussian Inc.: Pittsburgh, PA, 1995.
(43) Warshel, A.; Chu, Z. T.; Parson, W. W. *Science* **1989**, *246*, 112.
(44) Wikström, M. *Biochim. Biophys. Acta* **1998**, *1365*, 185−192. Karpenfors, M.; Ädelroth, P.; AAgaard, A.; Sigurdson, H.; Svenson Ek, M.; Brzezinski, P. *Biochim. Biophys. Acta* **1998**, *1365*, 159−169.
(45) Blomberg, M. R. A.; Siegbahn, P. E. M.; Babcock, G. T.; Wikström, M. Submitted for publication.
(46) Ferguson-Miller, S.; Babcock, G. T. *Chem. Rev.* **1996**, *96*, 2889−2907.
(47) Babcock, G. T.; Wikström, M. *Nature* **1992**, *356*, 301−309.
(48) Proshlyakov, D. A.; Ogura, T.; Shinzawa-Itoh, K.; Yoshikawa, S.; Kitagawa, T. *Biochemistry* **1996**, *35*, 76−78.
(49) Proshylakov, D. A.; Pressler, M. A.; Babcock, G. T. *Proc. Natl. Acad. Sci. U.S.A.* **1998**, *95*, 8020.
(50) Brzezinski, P. Private communication.
(51) Yoshioka, Y.; Kubo, S.; Yamaguchi, K.; Saito, I. *Chem. Phys. Lett.* **1998**, *294*, 459−467.
(52) Ghosh, A.; Skancke, A. *J. Phys. Chem. B* **1998**, *102*, 10087−10090.
(53) Yachandra, V. K.; Sauer, K.; Klein, M. P. *Chem. Rev.* **1996**, *96*, 2927−2950.
(54) (a) Hoganson, C. W.; Lydakis-Simantiris, N.; Tang, X.-S.; Tommos, C.; Warncke, K.; Babcock, G. T.; Diner, B. A.; McCracken, J.; Styring, S. *Photosynth. Res.* **1995**, *46*, 177. (b) Babcock, G. T. In *Photosynthesis from Light to Biosphere*; Mathis, P., Ed.; Kluwer: Dordrecht, 1995; Vol. 2, p 209. (c) Tommos, C.; Tang, X.-S.; Warncke, K.; Hoganson, C. W.; Styring, S.; McCracken, J.; Diner, B. A.; Babcock, G. T. *J. Am. Chem. Soc.* **1995**, *117*, 10325.
(55) (a) Renger, G. *Photosynthetica* **1987**, *21*,203−224. (b) Renger, G. *Physiol. Plant.* **1997**, *100*, 828−841.
(56) (a) Haumann, M.; Bögershausen, O.; Cherepanov, D.; Ahlbrink, R.; Junge, W. *Photosynth. Res.* **1997**, *51*, 193−208. (b) Ahlbrink, R.; Haumann, M.; Cherepanov, D.; Bögershausen, O.; Mulkidjanian, A.; Junge, W. *Biochemistry* **1998**, *37*, 1131−1142.
(57) Lindberg, K.; Andreasson, L. *Biochemistry* **1996**, *35*, 14259.
(58) Kok, B.; Forbush, B.; McGloin, M. *Photochem. Photobiol.* **1970**, *11*, 457.
(59) McGrady, J. E.; Stranger, R. *Inorg. Chem.* **1999**, *38*, 550−558.
(60) Cinco, R. M.; Robblee, J. H.; Rompel, A.; Fernandez, C.; Yachandra, V. K.; Sauer, K.; Klein, M. P. *J. Phys. Chem.* **1998**, *B102*, 8248−8256.
(61) Messinger, J.; Badger, M.; Wydrzinski, T. *Proc. Natl. Acad. Sci. U.S.A.* **1995**, *92*, 3209−3213.
(62) Howard, J. B.; Rees, D. C. *Chem. Rev.* **1996**, *96*, 2965−2982.
(63) Burgess, B. K.; Lowe, D. J. *Chem. Rev.*, **1996**, *96*, 2983−3011.
(64) Eady, R. R. *Chem. Rev.* **1996**, *96*, 3013−3030.
(65) Kim, J.; Rees, D. C. *Nature* **1992**, *360*, 553.
(66) Kim, J.; Rees, D. C. *Science* **1992**, *257*, 1677.
(67) Dean, D. R.; Bolin, J. T.; Zheng, L. M. *J. Bacteriol.* **1993**, *175*, 6737.
(68) Machado, B. C.; Davidson, E. R. *Theor. Chim. Acta* **1995**, *92*, 315−326.
(69) Siegbahn, P. E. M.; Svensson, M.; Westerberg, J.; Crabtree, R. H. *J. Phys. Chem.* **1998**, *B102*, 1615−1623.
(70) Rod, T. H.; Nørskov, J. K.; Hammer, B. *Phys. Rev. Lett.*, in press.
(71) Dance, I. *Chem. Commun.* **1998**, 523−530. Dance, I. *Chem. Commun.* **1997**, 165−166. Dance, I. G. *Aust. J. Chem.* **1994**, *47*, 979. Dance, I. G. *J. Biol. Inorg. Chem.* **1996**, *1*, 581.
(72) Volbeda, A.; Charon, M. H.; Piras, C.; Hatchikian, E. C.; Frey, M.; Fontecilla-Camps, J. C. *Nature* **1995**, *373*, 580. Volbeda, A.; Garcin, E.; Piras, C.; de Lacey, A. L.; Fernandez, V. M.; Hatchikian, E. C.; Frey, M.; Fontecilla-Camps, J. C. *J. Am. Chem. Soc.* **1996**, *118*, 12989.
(73) Happe, R. P.; Roseboom, W.; Pierik, A. J.; Albracht, S. P. J.; Bagley, K. A. *Nature* **1997**, *385*, 126.
(74) Pavlov, M.; Siegbahn, P. E. M.; Blomberg, M. R. A.; Crabtree, R. H. *J. Am. Chem. Soc.* **1998**, *120*, 548.
(75) Pavlov, M.; Blomberg, M. R. A.; Siegbahn, P. E. M. *Int. J. Quantum Chem.* **1999**, *73*, 197−207.
(76) Garcin, E.; Hatchikian, C.; Frey, M.; Fontecilla-Camps, J. C. private communication.
(77) Niu, S.; Thomson, L. M.; Hall, M. B. *J. Am. Chem. Soc.* **1999**, *121*, 4000−4007.
(78) Harris, D.; Loew, G. H. *J. Am. Chem. Soc.* **1998**, *120*, 8941−8948.
(79) Green, M. T. *J. Am. Chem. Soc.* **1999**, *121*, 7939−7940.
(80) Harris, D.; Loew, G.; Waskell, L. *J. Am. Chem. Soc.* **1998**, *120*, 4308−4318.
(81) Green, M. T. *J. Am. Chem. Soc.* **1998**, *120*, 10772−10773.
(82) Filatov, M.; Harris, N.; Shaik, S. *J. Chem. Soc., Perkin Trans. 2* **1999**, 399−410.
(83) Segall, M. D.; Payne, M. C.; Ellis, S. W.; Tucker, G. T.; Boyes, R. N. *Phys. Rev. E* **1998**, *57*, 4618−4621.
(84) Loew, G.; Harris, D. L. *Chem. Rev.* **2000**, *100*, 407−420.
(85) Wirstam, M.; Blomberg, M. R. A.; Siegbahn, P. E. M. *J. Am. Chem. Soc.* **1999**, *121*, 10178−10185.
(86) Kuramochi, H.; Noodleman, L.; Case, D. A. *J. Am. Chem. Soc.* **1997**, *119*, 11442−11451.
(87) Ghosh, A.; Almlöf, J.; Que, L. *J. Phys. Chem.* **1994**, *98*, 5576−5579.
(88) Deeth, R. T. *J. Am. Chem. Soc.* **1999**, *121*, 6074.
(89) Woon, D. E.; Loew, G. H. *J. Phys. Chem. A* **1998**, *98*, 10380−10384.
(90) Sigfridsson, E.; Ryde, U. *J. Biol. Inorg. Chem.* **1999**, *4*, 99−110.
(91) Vangberg, T.; Bocian, D.F. Ghosh, A. *J. Biol. Inorg. Chem.* **1997**, *2*, 526−530.
(92) Rovira, C.; Kunc, K.; Hutter, J.; Ballone, P.; Parrinello, M. *J. Phys. Chem. A* **1997**, *101*, 8914−8925.
(93) Ghosh, A.; Gonzalez, E.; Vangberg, T. *J. Phys. Chem. B* **1999**, *103*, 1363−1367.
(94) Ghosh, A.; Almlöf, J.; Que, L. *Angew. Chem.* **1996**, *35*, 770−772.
(95) Pietsch, M. A.; Hall, M. B. *Inorg. Chem.* **1996**, *35*, 1273−1278.
(96) Thapper, A.; Deeth, R. J.; Nordlander, E. *Inorg. Chem.* **1999**, *38*, 1015−1018.
(97) Mouesca, J.-M.; Chen, J. L.; Noodleman, L.; Bashford, D.; Case, D. A. *J. Am. Chem. Soc.* **1994**, *116*, 11898−11914.
(98) Li, J.; Nelson, M. R.: Peng, C. Y.; Bashford, D.; Noodleman, L. *J. Phys. Chem. A* **1998**, *102*, 6311−6324.
(99) Li, J.; Fisher, C. L.; Konecny, R.; Bashford, D.; Noodleman, L. *Inorg. Chem.* **1999**, *39*, 929−939.
(100) Konecny, R.; Li, J.; Fisher, C. L.; Dillet, V.; Bashford, D.; Noodleman, L. *Inorg. Chem.* **1999**, *39*, 940−50.
(101) Pierloot, K.; De Kerpel, J. O. A.; Ryde, U.; Roos, B. O. *J. Am. Chem. Soc.* **1997**, *119*, 218−226.
(102) Gewirth, A. A.; Solomon, E. I. *J. Am. Chem. Soc.* **1988**, *110*, 3811−3819.
(103) De Kerpel, J. O. A.; Pierloot, K.; Ryde, U.; Roos, B. O. *J. Phys. Chem.* **1998**, *102*, 4638−4647.

(104) Pierloot, K.; De Kerpel, J. O. A.; Ryde, U.; Olsson, M. H. M.; Roos, B. O. *J. Am. Chem. Soc.* **1998**, *120*, 13156−13166.
(105) Pierloot, K.; De Kerpel, J. O. A.; Ryde, U.; Roos, B. O. *J. Am. Chem. Soc.* **1997**, *119*, 218−226.
(106) Casida, M. E. In *Recent Advances in Density Functional Methods*; Chong, D. P., Ed.; World Scientific: Singapore, 1995; p 155.
(107) Tozer, D. J.; Amos, R. D.; Handy, N. C.; Roos, B. O.; Serrano-Andres, L., in press.
(108) Noodleman, L.; Li, J.; Zhao, X.-G.; Richardson, W. H. In *Methods in Chemistry and Materials Science*; Springborg, M., Ed.; John Wiley and Sons: New York, 1997; pp 149−187.
(109) Zhao, X. G.; Richardson, W. H.; Chen, J. L.; Li, J.; Noodleman, L.; Tsai, H.-L.; Hendrickson, D. N. *Inorg. Chem.* **1997**, *36*, 1198−217.
(110) Solomon, E. I.; Tuczek, F.; Root, D. E.; Brown, C. A. *Chem. Rev.* **1994**, *94*, 827−56.
(111) Tuczek, F.; Solomon, E. I. *J. Am. Chem. Soc.* **1994**, *116*, 6916−6924.
(112) Brown, C. A.; Remar, G. J.; Musselman, R. L.; Solomon, E. I. *Inorg. Chem.* **1995**, *34*, 688−717.

CR980390W